Int. J. Solids Structures Vol. 25, No. 8, pp. 901–916, 1989
Printed in Great Britain.

0020–7683/89 $3.00 + .00

NONDESTRUCTIVE EVALUATION OF INTERFACIAL DAMAGES IN COMPOSITE MATERIALS

ZHANJUN GAO and T. MURA
Department of Civil Engineering, Northwestern University, Evanston, IL 60201, U.S.A.

(*Received* 30 *March* 1988; *in revised form* 20 *December* 1988)

Abstract—The high stress concentration near the interface of fiber–matrix in composite materials causes the accumulation of the interfacial damages and the degradation of mechanical properties of the materials. In this paper, by using the residual surface displacement data, we evaluate the microscopic damages in terms of Somigliano's dislocations in composites near the interface caused by a series of unknown loadings. The goal of this research is to monitor the processes of the damage evolution near the interface and to relate this microscopic damage to the degradation of the macroscopic mechanical properties of the materials.

The problem is an inverse problem, which is substantially different from the conventional forward analysis of structural mechanics. Therefore, the uniqueness and stability must be considered. It is proved that the residual fields and all the characteristic quantities along the interface, such as displacement jumps (Somigliano's dislocations), are uniquely determined by the residual surface displacements. It follows that the traction free parts of the interface correspond to cracks, the normal displacement jumps indicate debonding and the tangential displacement jumps measure the interfacial sliding. A special technique is utilized to stabilize the numerical calculations.

1. INTRODUCTION

The local stresses are extremely large at the interface between fibers and matrix of composite materials when they are loaded. It is believed that these highly inhomogeneous stresses cause the accumulation of the damages near the interface of the materials, and relate directly to the degradation of the mechanical properties of the materials. Therefore, the evaluation of the interfacial damages in composite materials is very important in predicting the material failure.

Relations at the interface between the fields in fibers (inclusion) and those of the matrix are called interfacial conditions. In the conventional analysis of solid mechanics, the interfacial conditions are given beforehand. In Eshelby's (1957) problem of ellipsoidal inclusion, the interface is assumed to be perfect bonding, i.e. both normal and tangential displacements are continuous along the interface. This analysis has been extended to the sliding inclusion by Mura and Faruhashi (1984) and Mura *et al.* (1985). In their calculations it is assumed that the inclusion is free to slip along the interface and the normal displacement remains continuous. Other types of interfaces, such as the spring-type resistance model, have also been used to investigate the intermediate stage between perfect bonding and sliding inclusion (Lene and Leguillon, 1982). In any circumstance, the interfacial condition and all the loading and unloading history must be given to make the problem mathematically well defined.

The assumptions of perfect bonding, sliding and spring-type resistance etc. hold true for certain kinds of materials and loading stages. But as damages are accumulated along the interface due to the stress concentration, none of these assumptions is valid on the whole interface. Micro-cracks with different lengths and orientations are formed along the interface. The status of the interface varies from point to point. Some parts remain perfect bonding, while the other parts begin to debond or slide. The formation of the interfacial damages is really a very complicated process. It is difficult to make legitimate assumptions on the interfacial conditions especially when the loading and unloading history is uncertain. Therefore, the conventional analysis cannot be carried out to compute the stress field and to evaluate the degradation of the mechanical properties of the material.

The goal of this research is to evaluate the microscopic damages of interfaces caused by *unknown loadings*, by using the residual surface displacement data on the free surface of the material around an individual fiber, and to determine the internal degradation of the macroscopic material properties in terms of Somigliano's dislocations.

The residual surface displacements are obtained in the following way. One reference micrograph is taken before the material is put into usage. The other one is taken anytime when we want to evaluate the damages of the materials and all the loadings are removed. The residual surface displacements are relative and defined as the difference between the one in the second micrograph and the one in the first micrograph. We do not need to have any knowledge on the loading or unloading processes. If no damages have occurred, the two micrographs must be identical and therefore, the observed residual displacements are zero. If damages do occur along the interface, the residual surface displacements are nonzero. It is assumed that no damage occur in the fibers and the matrix, therefore, the observed residual displacements are caused by the interfacial damages. However, this assumption will be eliminated and the result will be reported in a separate paper.

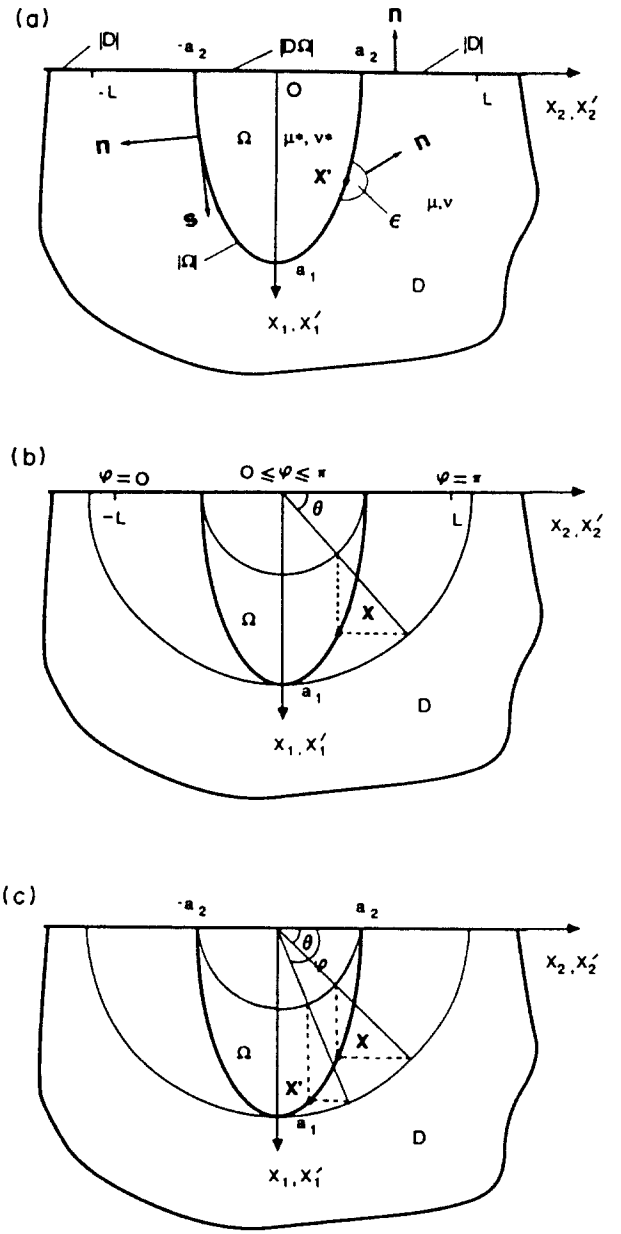

Fig. 1. (a) Half space $x_1 \geqslant 0$ is denoted by D. Ω is an inhomogeneity. Surface displacements in $x_2' \in [-L, L]$ are used to recover the interfacial quantities. $|D| = \{x_1 = 0, |x_2| \geqslant a_2\}$; $|D\Omega| = \{x_1 = 0, |x_2| < a_2\}$; $|\Omega| = \{x_1 \geqslant 0, x_1^2/a_1^2 + x_2^2/a_2^2 = 1\}$. (b) θ and φ for the transformation of (18a). $0 \leqslant \theta \leqslant \pi$ corresponds to x on the interface $|\Omega|$; $0 \leqslant \varphi \leqslant \pi$ corresponds to x′ on the interface $|\Omega|$. (c) θ and φ for the transformation of (18b). $0 \leqslant \theta \leqslant \pi$ corresponds to x on the interface $|\Omega|$; $0 \leqslant \varphi \leqslant \pi$ corresponds to x′ on the free surface $|D| + |D\Omega|$, i.e. $-L \leqslant x_2' \leqslant L$.

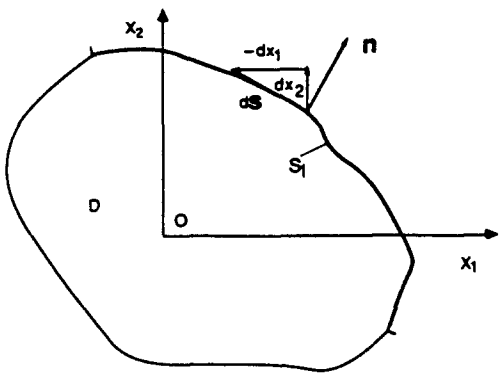

Fig. 2. Displacements and tractions are zero on S_1, a part of the boundary of D.

A unique set of experimental techniques has been developed to measure the surface displacements (Cox *et al.*, 1986). It is based on stereoscopic analysis of pairs of optical micrographs. The experimental measurements have high spatial resolution (0.1–100 μm) and high strain sensitivity (10^{-4} over 10 μm). Since a typical diameter of a fiber in composites is about several micrometers, these techniques can be employed to obtain the microscopic displacements around an individual fiber. Therefore, a composite material is modeled locally as a semi-ellipsoid inhomogeneity in a half space shown in Fig. 1(a). The inhomogeneity becomes a continuous fiber when a_1 approaches infinity.

The processes of cracking, sliding and debonding along the interface $|\Omega|$ are accompanied by localized plastic deformation or Somigliano's dislocations. Although the local stresses are high, the plastic strains occur only in a small layer near the interface. In this paper, as the first step to our goal, we replace the "damaged layer" by a distribution of Somigliano's dislocations

$$b_i(\mathbf{x}) = [u_i(\mathbf{x})], \quad \mathbf{x} \in |\Omega| \tag{1}$$

where [...] denote the displacement jumps.

In Fig. 1(a) the coordinate systems (x_1, x_2) and (x_1', x_2') coincide. Our problem is as follows.

By using the residual displacements on the free surface $-L \leqslant x_2' \leqslant L$, we evaluate $b_i(\mathbf{x})$ as well as $t_i(\mathbf{x})$, the tractions on the interface, by the use of the inverse method. Once $b_i(\mathbf{x})$ and $t_i(\mathbf{x})$ are found, the traction free parts of the interface correspond to cracks, the normal displacement jumps indicate debonding and the tangential displacement jumps measure the interfacial sliding. In the following section, it is proved that this inverse problem has a unique solution.

2. PROOF OF UNIQUENESS

The conventional forward analyses have been conducted extensively in the fields of science and engineering. On the other hand, inverse problems are inherently ill-posed. Definitive answers to questions of the existence, uniqueness and stability have been given only for a comparatively small class of inverse problems.

The following lemma is needed for the uniqueness of our problem.

Lemma. Let S_1 be a part of the boundary of a two-dimensional† elastic body D (see Fig. 2). If there are no body forces and

† The lemma holds for the three-dimensional case. A reviewer of this paper hinted its proof by use of the Betti's reciprocal theorem. According to Muskhelshvili's book, Almansi (1907) proved that.

$$u_i = 0 \quad \text{on } S_1 \tag{2}$$

$$t_i = 0 \quad \text{on } S_1 \tag{3}$$

where u_i, t_i are the displacements and tractions, respectively, then $u_i = 0$, $\sigma_{ij} = 0$ in the entire domain of the body D.

The proof of the lemma was given by the book of Muskhelshvili (1963).†

Now we can prove the uniqueness of the problem in Fig. 1(a). Consider the domain D–Ω and assume that the two states of displacements u_i^1, u_i^2 and stresses σ_{ij}^1, σ_{ij}^2 give the same surface displacements and zero surface tractions on $-L \leqslant x_2' \leqslant L$. Then, the difference fields

$$u_i = u_i^1 - u_i^2 \quad \text{and } \sigma_{ij} = \sigma_{ij}^1 - \sigma_{ij}^2$$

of course satisfy zero tractions and zero displacements on the sub-surface $-L \leqslant x_2' \leqslant -a_2$ and $a_2 \leqslant x_2' \leqslant L$, which is the S_1 boundary of D–Ω. Therefore, from the above lemma, we obtained

$$u_i = 0 \text{ and } \sigma_{ij} = 0 \quad \text{in } D\text{–}\Omega,$$

that is

$$u_i^1 = u_i^2 \text{ and } \sigma_{ij}^1 = \sigma_{ij}^2 \quad \text{in } D\text{–}\Omega.$$

It should be emphasized that the lemma holds regardless of the boundary condition on $|\Omega|$ since S_1 in the lemma is only a part of the boundary not the whole boundary.

Similarly, we can prove

$$u_i^1 = u_i^2 \text{ and } \sigma_{ij}^1 = \sigma_{ij}^2 \quad \text{in } \Omega.$$

This completes the proof of the uniqueness for the problem stated in the end of the last section.

3. FORMATION OF THE PROBLEM

Let us derive the integral equation for the problem. The configuration is shown in Fig. 1(a). Let $u_i(\mathbf{x})$ be the residual displacements in the domain D, caused by interfacial dislocations of the material. $\mathbf{x}$ represents any field point in D. Choose another fixed point in D, which is denoted by $\mathbf{x}'$ to distinguish it from $\mathbf{x}$. Now we derive the integral equations which relate the field quantities at $\mathbf{x}$ to those at $\mathbf{x}'$.

Consider the domain occupied by the matrix. The small domain ε is chosen to exclude the point $\mathbf{x}'$ from the integration domain D–Ω.

Due to the symmetry of the material constant tensor C_{ijkl} we have

$$C_{ijkl}G_{km,l}(\mathbf{x}, \mathbf{x}')u_{i,j}(\mathbf{x}) = C_{ijkl}G_{im,j}(\mathbf{x}, \mathbf{x}')u_{k,l}(\mathbf{x}) \tag{4}$$

where $G_{km}(\mathbf{x}, \mathbf{x}')$ is Green's function in the half space, with elastic moduli C_{ijkl}. That is, $G_{km}(\mathbf{x}, \mathbf{x}')$ is the displacement at point $\mathbf{x}$ in the x_k direction due to a unit force at point $\mathbf{x}'$ in the x_m' direction. $G_{km,l}(\mathbf{x}, \mathbf{x}')$ indicates $(\partial/\partial x_l)G_{km}(\mathbf{x}, \mathbf{x}')$. The expression of the Green's function can be found in Dundurs (1962),

$$G_{ij}(\mathbf{x}, \mathbf{x}') = G_{ij}^{(1)}(\mathbf{x}, \mathbf{x}') + G_{ij}^{(2)}(\mathbf{x}, \mathbf{x}') \tag{5a}$$

where

† Ibid.

$$G_{ij}^{(1)}(\mathbf{x},\mathbf{x}') = \frac{1}{2\pi\mu(1+\nu)}\{-\kappa\delta_{ij}\log(R_1)+(x_i-x_i')(x_j-x_j')/R_1^2\} \tag{5b}$$

is Green's function for the infinite medium

$$\delta_{ij} = \begin{cases} 0 & \text{when } i \neq j \\ 1 & \text{when } i = j \end{cases}$$

$$R_1^2 = (x_1-x_1')^2+(x_2-x_2')^2$$

and

$$G_{11}^{(2)}(\mathbf{x},\mathbf{x}') = \frac{1}{4\pi\mu(1+\kappa)}\{-(1+\kappa^2)\log(R_2)+2\kappa(x_1+x_1')^2/R_2^2+2x_1'[-2(x_1+x_1')/R_2^2 + 4(x_1+x_1')^3/R_2^4-2x_1'(2(x_1+x_1')^2/R_2^4-1/R_2^2)]\}$$

$$G_{22}^{(2)}(\mathbf{x},\mathbf{x}') = \frac{1}{4\pi\mu(1+\kappa)}\{-(1+\kappa^2)\log(R_2)-2\kappa(x_1+x_1')^2/R_2^2 - 2x_1'[2(x_1+x_1')/R_2^2-4x_1(x_1+x_1')^2/R_2^4-2x_1'/R_2^2]\}$$

$$G_{12}^{(2)}(\mathbf{x},\mathbf{x}') = \frac{1}{4\pi\mu(1+\kappa)}\{(-1+\kappa^2)\tan^{-1}[(x_2-x_2')/(x_1+x_1')]+2\kappa(x_1+x_1')(x_2-x_2')/R_2^2 - 2x_1'[2\kappa(x_2-x_2')/R_2^2+4x_1(x_1+x_1')(x_2-x_2')/R_2^4]\}$$

$$G_{21}^{(2)}(\mathbf{x},\mathbf{x}') = \frac{1}{4\pi\mu(1+\kappa)}\{(1-\kappa^2)\tan^{-1}[(x_2-x_2')/(x_1+x_1')]+2\kappa(x_1+x_1')(x_2-x_2')/R_2^2 + 2x_1'[-2\kappa(x_2-x_2')/R_2^2+4x_1(x_1+x_1')(x_2-x_2')/R_2^4]\} \tag{5c}$$

where

$$R_2^2 = (x_1+x_1')^2+(x_2-x_2')^2.$$

The Green's function in the half space, with elastic moduli C_{ijkl}^* is

$$G_{ij}^*(\mathbf{x},\mathbf{x}') = G_{ij}^{(1)*}(\mathbf{x},\mathbf{x}')+G_{ij}^{(2)*}(\mathbf{x},\mathbf{x}') \tag{5d}$$

where the expressions of $G_{ij}^{(1)*}(\mathbf{x},\mathbf{x}')$ and $G_{ij}^{(2)*}(\mathbf{x},\mathbf{x}')$ follow from those in (5b) and (5c) by replacing μ, ν with μ^*, ν^*, respectively.

When (4) is integrated in domain D–Ω–ε with respect to x and Gauss's theorem is applied, we obtain

$$\begin{aligned}
&\int_{|D|} C_{ijkl}G_{km,l}(\mathbf{x},\mathbf{x}')u_i(\mathbf{x})n_j(\mathbf{x})\,ds(\mathbf{x}) - \int_{|\Omega|} C_{ijkl}G_{km,l}(\mathbf{x},\mathbf{x}')u_i(\mathbf{x})n_j(\mathbf{x})\,ds(\mathbf{x}) \\
&- \int_{|\varepsilon|} C_{ijkl}G_{km,l}(\mathbf{x},\mathbf{x}')u_i(\mathbf{x})n_j(\mathbf{x})\,ds(\mathbf{x}) - \int_{D-\Omega-\varepsilon} C_{ijkl}G_{km,lj}(\mathbf{x},\mathbf{x}')u_i(\mathbf{x})\,d\mathbf{x} \\
&= \int_{|D|} C_{ijkl}G_{im}(\mathbf{x},\mathbf{x}')u_{k,l}(\mathbf{x})n_j(\mathbf{x})\,ds(\mathbf{x}) - \int_{|\Omega|} C_{ijkl}G_{im}(\mathbf{x},\mathbf{x}')u_{k,l}(\mathbf{x})n_j(\mathbf{x})\,ds(\mathbf{x}) \\
&- \int_{|\varepsilon|} C_{ijkl}G_{im}(\mathbf{x},\mathbf{x}')u_{k,l}(\mathbf{x})n_j(\mathbf{x})\,ds(\mathbf{x}) - \int_{D-\Omega-\varepsilon} C_{ijkl}G_{im}(\mathbf{x},\mathbf{x}')u_{k,lj}(\mathbf{x})\,d\mathbf{x}
\end{aligned} \tag{6}$$

where $n_j(\mathbf{x})$ is the outer normal shown in Fig. 1(a), and $|D|$ is also defined in Fig. 1(a).

The boundary conditions and equilibrium for Green's function give

$$C_{ijkl}G_{km,l}(\mathbf{x},\mathbf{x}')n_j(\mathbf{x}) = 0 \quad \text{for } \mathbf{x} \text{ on } |D|$$
$$C_{ijkl}G_{km,lj}(\mathbf{x},\mathbf{x}') = 0 \quad \text{for } \mathbf{x} \text{ in } D\text{–}\Omega\text{–}\varepsilon \tag{7}$$

and the boundary conditions and equilibrium for field $u_i(\mathbf{x})$ are

$$C_{ijkl}u_{k,l}(\mathbf{x})n_j(\mathbf{x}) = 0 \quad \text{for } \mathbf{x} \text{ on } |D|$$
$$C_{ijkl}u_{k,lj}(\mathbf{x}) = 0 \quad \text{for } \mathbf{x} \text{ in } D\text{–}\Omega\text{–}\varepsilon. \tag{8}$$

When ε approaches to zero we have

$$\lim_{\varepsilon\to 0}\int_{|\varepsilon|} C_{ijkl}G_{km,l}(\mathbf{x},\mathbf{x}')n_j(\mathbf{x})\,ds(\mathbf{x}) = -\beta\delta_{im} \tag{9}$$

where

$$\beta = \begin{cases} 0 & \text{when } \mathbf{x}' \text{ on } |D\Omega| \\ 0.5 & \text{when } \mathbf{x}' \text{ on } |\Omega| \\ 1 & \text{when } \mathbf{x}' \text{ on } |D| \end{cases}$$

and

$$\lim_{\varepsilon\to 0}\int_{|\varepsilon|} C_{ijkl}G_{im}(\mathbf{x},\mathbf{x}')u_{k,l}(\mathbf{x})n_j(\mathbf{x})\,ds(\mathbf{x}) = 0. \tag{10}$$

Equation (10) follows from the fact that Green's function behaves like $\log(R_1)$ near its singularities and (9) can be evaluated directly from the expression of the Green's function.

Using (7)–(10) and letting ε approach to zero, we can write (6) as

$$-\beta u_m(\mathbf{x}') + \int_{|\Omega|} C_{ijkl}G_{km,l}(\mathbf{x},\mathbf{x}')u_i(\mathbf{x})n_j(\mathbf{x})\,ds(\mathbf{x}) - \int_{|\Omega|} t_i(\mathbf{x})G_{im}(\mathbf{x},\mathbf{x}')\,ds(\mathbf{x}) = 0 \tag{11}$$

where $t_i(\mathbf{x}) = C_{ijkl}u_{k,l}(\mathbf{x})n_j(\mathbf{x})$ are the tractions on the interface.

The integral equations for the inhomogeneity Ω have the form similar to (11) with C_{ijkl} and G_{ij} replaced by C^*_{ijkl} and G^*_{ij}, respectively, and the sign of $n_j(\mathbf{x})$ is taken properly. These equations are

$$\beta^* u^*_m(\mathbf{x}') + \int_{|\Omega|} C^*_{ijkl}G^*_{km,l}(\mathbf{x},\mathbf{x}')u^*_i(\mathbf{x})n_j(\mathbf{x})\,ds(\mathbf{x}) - \int_{|\Omega|} t_i(\mathbf{x})G^*_{im}(\mathbf{x},\mathbf{x}')\,ds(\mathbf{x}) = 0 \tag{12}$$

where

$$\beta^* = \begin{cases} 1 & \text{when } \mathbf{x}' \text{ on } |D\Omega| \\ 0.5 & \text{when } \mathbf{x}' \text{ on } |\Omega| \\ 0 & \text{when } \mathbf{x}' \text{ on } |D| \end{cases}$$

and

$$t_i(\mathbf{x}) = C^*_{ijkl}u^*_{k,l}(\mathbf{x})n_j(\mathbf{x}) = C_{ijkl}u_{k,l}(\mathbf{x})n_j(\mathbf{x})$$

means that tractions are continuous along the interface. $|D\Omega|$ is defined in Fig. 1(a).

We define the interfacial displacement jumps as

$$b_i(\mathbf{x}) = u_i^*(\mathbf{x}) - u_i(\mathbf{x}). \tag{13}$$

Our purpose is to determine $u_i(\mathbf{x})$, $t_i(\mathbf{x})$ and $b_i(\mathbf{x})$ from the residual surface displacements on $-L \leqslant x_2' \leqslant L$.

When $\mathbf{x}'$ is on $|\Omega|$, (11) and (12) yield

$$-0.5u_m(\mathbf{x}') + \int_{|\Omega|} C_{ijkl}G_{km,l}(\mathbf{x}, \mathbf{x}')u_i(\mathbf{x})n_j(\mathbf{x})\,ds(\mathbf{x}) - \int_{|\Omega|} t_i(\mathbf{x})G_{im}(\mathbf{x}, \mathbf{x}')\,ds(\mathbf{x}) = 0 \tag{14}$$

$$0.5[b_m(\mathbf{x}') + u_m(\mathbf{x}')] + \int_{|\Omega|} C^*_{ijkl}G^*_{km,l}(\mathbf{x}, \mathbf{x}')[b_i(\mathbf{x}) + u_i(\mathbf{x})]n_j(\mathbf{x})\,ds(\mathbf{x}) - \int_{|\Omega|} t_i(\mathbf{x})G^*_{im}(\mathbf{x}, \mathbf{x}')\,ds(\mathbf{x}) = 0. \tag{15}$$

For any $\mathbf{x}'$ on the free surface $-L \leqslant x_2' \leqslant L$, (11) and (12) become

$$\int_{|\Omega|} C_{ijkl}G_{km,l}(\mathbf{x}, \mathbf{x}')u_i(\mathbf{x})n_j(\mathbf{x})\,ds(\mathbf{x}) - \int_{|\Omega|} t_i(\mathbf{x})G_{im}(\mathbf{x}, \mathbf{x}')\,ds(\mathbf{x}) = \begin{cases} u^t_m(\mathbf{x}') & \text{for } \mathbf{x}' \text{ on } |D| \\ 0 & \text{for } \mathbf{x}' \text{ on } |D\Omega| \end{cases} \tag{16}$$

$$\int_{|\Omega|} C^*_{ijkl}G^*_{km,l}(\mathbf{x}, \mathbf{x}')[b_i(\mathbf{x}) + u_i(\mathbf{x})]n_j(\mathbf{x})\,ds(\mathbf{x}) - \int_{|\Omega|} t_i(\mathbf{x})G^*_{im}(\mathbf{x}, \mathbf{x}')\,ds(\mathbf{x}) = \begin{cases} -u^t_m(\mathbf{x}') & \text{for } \mathbf{x}' \text{ on } |D\Omega| \\ 0 & \text{for } \mathbf{x}' \text{ on } |D| \end{cases}. \tag{17}$$

Equations (14)–(17) determine the six interfacial quantities u_i, t_i and b_i from the known surface displacements $u^t_m(\mathbf{x}')$ on $-L \leqslant x_2' \leqslant L$. There are in total *eight equations* in (14)–(17) (since $m = 1, 2$), with *six unknowns*. This indicates the ill-posed nature of the inverse problem.

By employing transformation of variables [see Fig. 1(b and c)]

$$\begin{aligned} &x_1 = a_1 \sin\theta, \quad x_2 = a_2 \cos\theta \\ &x_1' = a_1 \sin\varphi, \quad x_2' = a_2 \cos\varphi, \quad \mathbf{x}, \mathbf{x}' \text{ on } |\Omega|, \quad 0 \leqslant \varphi, \theta \leqslant \pi \end{aligned} \tag{18a}$$

for (14) and (15), and

$$\begin{aligned} &x_1 = a_1 \sin\theta, \quad x_2 = a_2 \cos\theta, \\ &x_1' = 0, \quad x_2' = \frac{2L}{\pi}\varphi - L, \quad \mathbf{x}, \mathbf{x}' \text{ on } |\Omega| + |D\Omega|, \quad 0 \leqslant \varphi, \theta \leqslant \pi \end{aligned} \tag{18b}$$

for (16) and (17), we can write (14)–(17) as (see Appendix A)

$$\int_0^{\pi} \mathbf{K}(\theta, \varphi)\mathbf{V}(\theta)\,\mathrm{d}\theta = \mathbf{U}(\varphi), \quad 0 \leqslant \varphi \leqslant \pi. \tag{19}$$

where $\mathbf{K}(\theta, \varphi)$ is an 8 by 6 matrix given in (A13) and $\mathbf{V}(\theta)$ and $\mathbf{U}(\varphi)$ are

$$\mathbf{V}(\theta) = [u_1(\theta), u_2(\theta), t_1(\theta), t_2(\theta), b_1(\theta), b_2(\theta)]^T \tag{20}$$

$$\mathbf{U}(\varphi) = [0, 0, 0, 0, 0, 0, -u_1^s(\varphi), -u_2^s(\varphi)]^T, \quad \text{for } \varphi \in [(L-a_2)\pi/2L, (L+a_2)\pi/2L]$$
$$\mathbf{U}(\varphi) = [0, 0, 0, 0, u_1^s(\varphi), u_2^s(\varphi), 0, 0]^T, \quad \text{for } \varphi \notin [(L-a_2)\pi/2L, (L+a_2)\pi/2L]. \tag{21}$$

The nature of θ and φ is indicated in Fig. 1(b and c).

Equation (19) is an integral equation for $\mathbf{V}(\theta)$. If we can solve (19) for $\mathbf{V}(\theta)$ by using given $\mathbf{U}(\varphi)$, the surface displacements, we obtain all the characteristic quantities on the interface. However, there are two difficulties remaining.

The first one is the instability. The stability of a problem refers to the influence of the error of the input data on the perturbation of the solution. In (19) the right hand term $\mathbf{U}(\varphi)$ comes from the experimental measurements. $\mathbf{U}(\varphi)$ is an approximation of $\mathbf{U}^0(\varphi)$, the real surface displacements. The accuracy of these data is estimated by the following expression

$$\|\mathbf{U}(\varphi) - \mathbf{U}^0(\varphi)\|^2 \leqslant \varepsilon \tag{22}$$

where $\|\ldots\|$ is L_2 norm, that is

$$\|\mathbf{U}(\varphi)\|^2 = \int_0^{\pi} \mathbf{U}^T(\varphi)\mathbf{U}(\varphi)\,\mathrm{d}\varphi \tag{23}$$

and $\mathbf{U}^T(\varphi)$ is the transpose of $\mathbf{U}(\varphi)$. The stability of the problem states that, as the experimental data $\mathbf{U}(\varphi)$ are sufficiently close to the exact data $\mathbf{U}^0(\varphi)$ (i.e. $\varepsilon \ll 1$), the solution $\mathbf{V}(\theta)$ of (19) should be very close to the exact solution of the problem.

It is believed that most mathematical problems corresponding to physical phenomena are stable. However, inverse problems are generally unstable. Although we have proved the uniqueness of the problem in Fig. 1(a), due to the ill-posed nature of the Fredholm integral equation of the first kind, Gao and Mura (1989a) and Mura *et al.* (1986), eqn (19) is extremely unstable. Even though $\mathbf{U}(\varphi)$ deviates only slightly from $\mathbf{U}^0(\varphi)$, the solution of (19) defers greatly from the exact solution.

The other difficulty is that (19) has eight equations with six unknowns. It cannot be solved numerically in a conventional way. Therefore, special consideration must be taken.

4. METHOD OF SOLUTIONS

The so called "regularization method" was suggested by Tikhonov (1963) to solve one-dimensional Fredholm integral equations of the first kind with regular kernel. Such equations are numerically unstable. The regularization method is based on the radical idea that the stability can be attained by narrowing the class of possible solutions through the introduction of an auxiliary positive definite functional. Gao and Mura (1989a) have utilized the regularization method in their calculations of residual plastic strains.

A new well-posed problem related to (19) is derived in the following way.

Since problem (19) has the unique solution, it is equivalent to the following variational problem

$$\text{Min} \|\mathbf{V}(\theta)\|^2$$

$$\text{Subject to} \left\| \int_0^{\pi} \mathbf{K}(\theta, \varphi)\mathbf{V}(\theta)\,\mathrm{d}\theta - \mathbf{U}(\varphi) \right\|^2 = 0 \tag{24}$$

where the norms follow the definition in (23).

Since $\mathbf{U}(\varphi)$ is the ε-approximation of surface displacements, according to (22), the variational problem (24) is further modified as

$$\text{Min} \|\mathbf{V}(\theta)\|^2$$

$$\text{Subject to} \left\| \int_0^{\pi} \mathbf{K}(\theta, \varphi)\mathbf{V}(\theta)\,\mathrm{d}\theta - \mathbf{U}(\varphi) \right\|^2 = \varepsilon. \tag{25}$$

Problem (25) is equivalent to

$$\text{Min} \left\{ \|\mathbf{V}(\theta)\|^2 + \lambda \left[\left\| \int_0^{\pi} \mathbf{K}(\theta, \varphi)\mathbf{V}(\theta)\,\mathrm{d}\theta - \mathbf{U}(\varphi) \right\|^2 - \varepsilon \right] \right\} \tag{26}$$

where λ is a Lagrange multiplier.

Let $\alpha = 1/\lambda$, we can write (26) as

$$\text{Min} \left\{ \alpha \|\mathbf{V}(\theta)\|^2 + \lambda \left[\left\| \int_0^{\pi} \mathbf{K}(\theta, \varphi)\mathbf{V}(\theta)\,\mathrm{d}\theta - \mathbf{U}(\varphi) \right\|^2 - \varepsilon \right] \right\}. \tag{27}$$

The Euler equation of (27) is

$$\int_0^{\pi} \mathbf{K}^*(\theta, \phi)\mathbf{V}(\theta)\,\mathrm{d}\theta + \alpha\mathbf{V}(\phi) = \mathbf{U}^*(\phi) \quad \phi \in [0, \pi] \tag{28a}$$

and α is a positive parameter determined by

$$f(\alpha) = 0, \tag{28b}$$

with

$$f(\alpha) = \left\| \int_0^{\pi} \mathbf{K}(\theta, \varphi)\mathbf{V}^{\alpha}(\theta)\,\mathrm{d}\theta - \mathbf{U}(\varphi) \right\|^2 - \varepsilon$$

where $\mathbf{V}^{\alpha}(\theta)$ is the solution of (28a) and

$$\mathbf{K}^*(\theta, \phi) = \int_0^{\pi} \mathbf{K}^T(\phi, \varphi)\mathbf{K}(\theta, \varphi)\,\mathrm{d}\varphi \quad \phi \in [0, \pi] \tag{28c}$$

$$\mathbf{U}^*(\phi) = \int_0^{\pi} \mathbf{K}^T(\phi, \varphi)\mathbf{U}(\varphi)\,\mathrm{d}\varphi \quad \phi \in [0, \pi]. \tag{28d}$$

$\mathbf{K}^T(\phi, \varphi)$ is the transpose of the matrix $\mathbf{K}(\phi, \varphi)$.

Equation (28a) is a Fredholm integral equation of the second kind with a self-adjoint kernel $\mathbf{K}^*(\theta, \phi)$. It is a typical well-posed problem. It can be proved that the solution of (28a) is stable for the small perturbation of the measurement term $\mathbf{U}(\varphi)$. That is, when ε in (22) is sufficiently small, the solution of (28a) is a very good approximation of the exact

solution of the problem. More detailed discussions can be found in the authors' publication, Gao and Mura (1989).

5. NUMERICAL CALCULATIONS

Equation (28a) is the new equation derived from our original problem (19). The parameter α in (28a) satisfies the nonlinear equation (28b). For any chosen α, equation (28a) can be solved by using conventional techniques. An iteration procedure should be used to adjust α such that equation (28b) is also satisfied.

There is no general method for solving nonlinear equations. Depending upon the equation we deal with, the iteration procedure may not converge. Fortunately, it can be shown (see Appendix B) that $f(\alpha)$ is an increasing function and

$$\lim_{\alpha \to 0^+} f(\alpha) < 0 \tag{29}$$

and

$$\lim_{\alpha \to +\infty} f(\alpha) > 0. \tag{30}$$

Therefore, the following convergent algorithm is constructed.

Step 1: ε is chosen from our knowledge on the accuracy of the displacement data.
Step 2: Compute $\mathbf{K}^*(\theta, \phi)$, $\mathbf{U}^*(\phi)$ from (28c) and (28d).
Step 3: Let δ be a given small positive number for convergence criterion. Choose positive numbers α_1 and α_2 such that $\alpha_1 < \alpha_2$, and

$$f(\alpha_1) < 0, \quad f(\alpha_2) > 0.$$

Step 4: Choose $\alpha = (\alpha_1 + \alpha_2)/2$ and solve (28a) again.
If $|f(\alpha)| < \delta$ then take $\mathbf{V}^2(\theta)$ as the solution and stop, else go to Step 5.
Step 5: If $f(\alpha) > 0$, let $\alpha_1 = \alpha_1$, $\alpha_2 = \alpha$, else let $\alpha_1 = \alpha$, $\alpha_2 = \alpha_2$.
Go to Step 4.

In the Step 4, equation (28a) is solved in the following way.
The interval $[0, \pi]$ is divided into ten equal length elements:

$$\mathbf{E}_i = \left[\frac{\pi}{10}(i-1), \frac{\pi}{10} i\right], \quad i = 1, 2, \ldots, 10.$$

$\mathbf{V}^2(\theta)$ is considered as a constant in $\mathbf{E}_i$, i.e.

$$\mathbf{V}^2(\theta) = \mathbf{V}^2(\theta_i), \quad \text{for } \theta \in \mathbf{E}_i$$

where

$$\theta_i = \frac{\pi}{10} i - \frac{\pi}{20}, \quad i = 1, 2, \ldots, 10.$$

When ϕ is chosen as

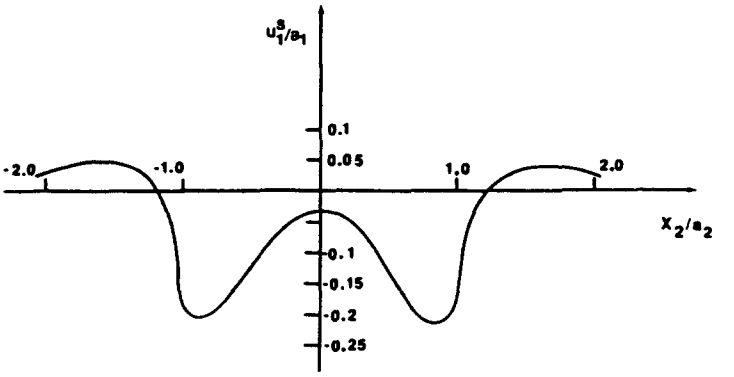

Fig. 3. Surface displacement, u_1^s, used to compute the interfacial damages.

$$\frac{\pi}{10}j-\frac{\pi}{20} \quad \text{for } j=1,2,\ldots,10,$$

eqn (28a) yields to a system of algebraic equations, which can be solved for $V^*(\theta_i)$, $i=1,2,\ldots,10$.

As we have mentioned in the introduction, the stereoscopic analyses of optical micrographs have high spatial resolution and high strain sensitivity, which enable us to measure the microscopic surface displacements around an individual fiber. When these measured surface displacements are used in (28a), we can evaluate the interfacial damage quantities $u_1(\theta)$, $u_2(\theta)$, $t_1(\theta)$, $t_2(\theta)$, $b_1(\theta)$, $b_2(\theta)$.

An example is presented here to demonstrate our method. The configuration is shown in Fig. 1(a) with $L=\pi/2$, $a_1=1.0$, $a_2=0.942$, $\mu^*=16.15$ GPa, $\nu^*=0.3$, $\mu=12.8$ GPa and $\nu=0.25$.

After a series of unknown loadings, damages are accumulated along the interface. Our purpose is to determine the quantities $u_1(\theta)$, $u_2(\theta)$, $t_1(\theta)$, $t_2(\theta)$, $b_1(\theta)$, $b_2(\theta)$ on the interface by using surface displacement data and solving (28a).

In this example, to test the method and make comparison, u_i^s is taken the same as the surface displacements caused by interfacial sliding dislocations (no debonding)

$$\begin{aligned} b_1(\theta) &= -a_2a_1^2\sin\theta\cos^2\theta/\{[a_2\sin\theta]^2+[a_1\cos\theta]^2\}^{1.5} \\ b_2(\theta) &= a_1a_2^2\cos\theta\sin^2\theta/\{[a_2\sin\theta]^2+[a_1\cos\theta]^2\}^{1.5} \end{aligned} \tag{31}$$

and therefore we can compare the numerical results with those caused by the dislocations in (31). θ is defined in (18) and shown in Fig. 1(b). The displacement and stress fields caused by (31) can be calculated easily since it is a well posed forward problem. In applying the method to a practical problem, however, we need to obtain the data from experiment. The surface displacements u_i^s are shown in Fig. 3 and Fig. 4. These residual surface displacements

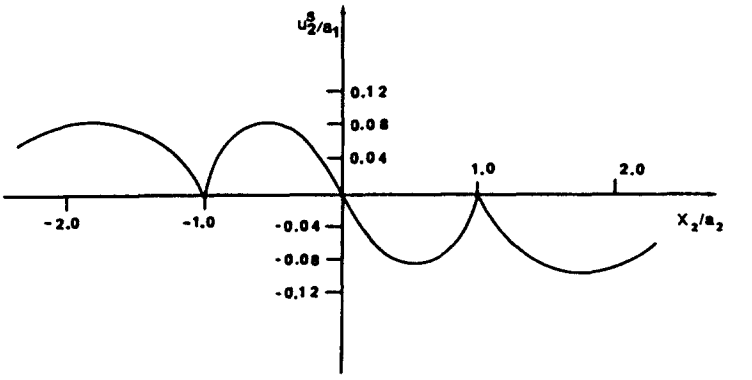

Fig. 4. Surface displacement, u_2^s, used to compute the interfacial damages.

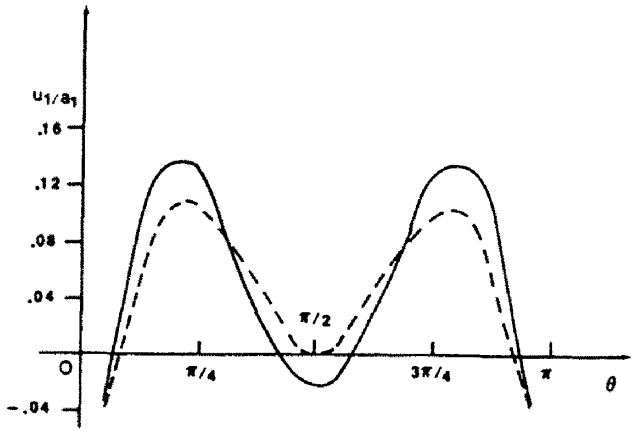

Fig. 5. Displacement u_1 on the interface (in matrix side). Dashed line is the exact solution. Solid line is the numerical result. θ is shown in Fig. 1(b and c).

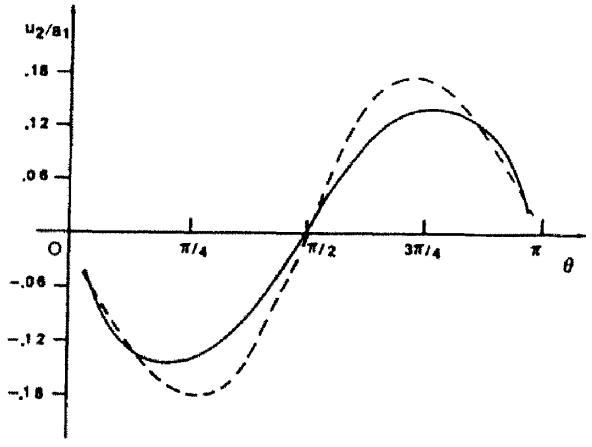

Fig. 6. Displacement u_2 on the interface (in matrix side). Dashed line is the exact solution. Solid line is the numerical result.

have error comparing with the exact surface displacements caused by the dislocation in (31). The ε in (22), which measures this error, is of order of 10^{-5}.

In the numerical calculations, the algorithm described in the beginning of this section is utilized. Figures 5–9 show the comparison of numerical results (solid lines) to the exact solution [dashed lines, caused by (31)]. The positive directions of **n** and **s** are given in Fig. 1(a). The final value of α is 0.0000008.

The numerical calculations show that the computed normal displacement jump is negligibly small and the tractions vanish only at some points (not a part) of the interface. Therefore we conclude that no cracking or debonding has happened along the interface. Tangential interface sliding does occur and its distribution is shown in Fig. 9.

6. CONCLUSION

In this paper we present a method for the nondestructive evaluation of the interfacial damages in composite materials. It has been proved that the residual fields and therefore all the characteristic quantities along the interface such as the displacement jumps $[u_i(\theta)]$ and the tractions $t_i(\theta)$, are uniquely determined by the residual surface displacements. It

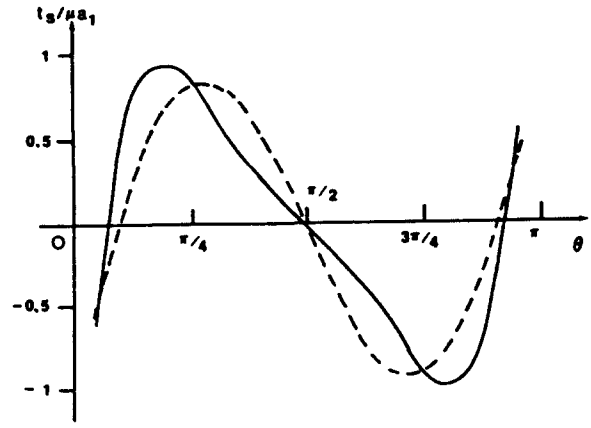

Fig. 7. Tangential traction t_s on the interface. Dashed line is the exact solution. Solid line is the numerical result.

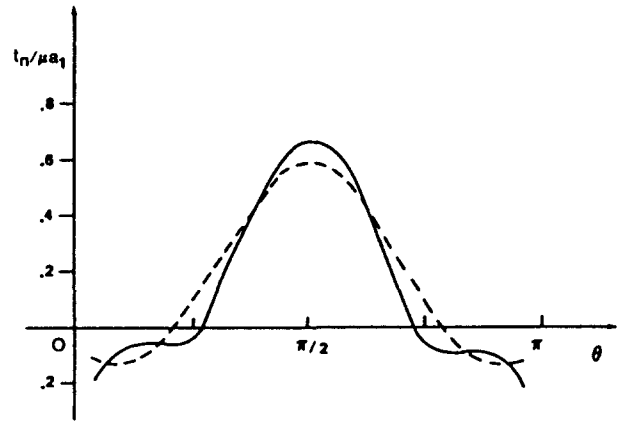

Fig. 8. Normal traction t_n on the interface. Dashed line is the exact solution. Solid line is the numerical result.

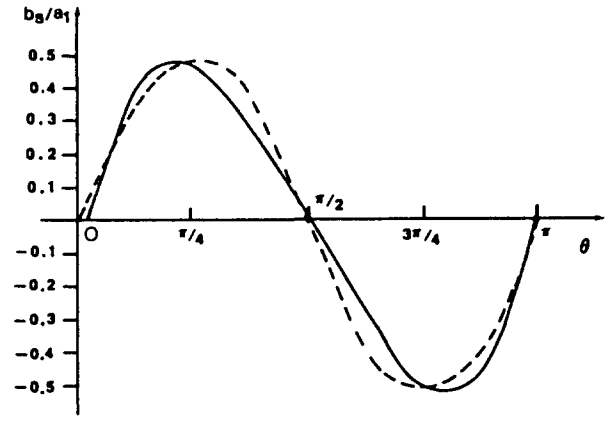

Fig. 9. Displacement jump b_s on the interface. Dashed line is the exact solution. Solid line is the numerical result.

follows that the traction free parts of the interface correspond to cracking, the normal displacement jumps indicate debonding and the tangential displacement jumps measure the interfacial sliding. It is clear that the residual surface displacement data do contain very important information about the damages inside the materials. Once an appropriate algorithm is employed, we can extract the information from these data. The key point is that the conventional numerical techniques cannot be used directly in such inverse problems.

When we seek a numerical solution, we should pay special attention to the stability of the problem. The method we presented in this paper can be employed for such a purpose.

The problem of evaluating the localized plastic damages has also been considered, (Gao and Mura, 1989a,b). It is shown that, although the residual surface displacements are not sufficient to recover the shape of the damage domain and the exact distribution of the residual plastic strains, some important characteristic quantities associated with the dislocations of the material can be obtained. These quantities include stresses in the vicinity of the damage domain, lower bounds of the strain energy or any other quadratic functions of the plastic strains. By using the obtained characteristic quantities and some constitutive models on the local plastic deformations, we can examine closely the localized microscopic plastic deformation near the interface, and relate the local damages to the degradation of macroscopic material properties.

The residual surface displacements serve as sensors for the damages inside the materials. The coordination and feedback among experimental measurements, constitutive model and evaluation of plastic deformation by surface displacement data enable us to elucidate the relationship between the current condition of the interface and the rate of accumulation of plastic damages due to any unknown loadings. All sorts of inverse or semi-inverse problems can be solved in a similar approach.

Acknowledgement—This research was supported by Rockwell Science Center DAAL03-88-C-0027.

REFERENCES

Almansi, E. (1907). Un teorema sulle deformazioni elastiche dei solidi isotropi. *Rendic. del Circolo Mat. di Palermo, 5th ser.* **XVI**, 865–868.

Cox, B., Morris, W. and James, M. (1986). High sensitivity, high spatial resolution strain measurements in alloys and composites. *Proc. Conf. on Nondestructive Testing and Evaluations of Advanced Materials and Composites*, Colorado Springs, CO.

Dundurs, J. (1962). Force in smoothly joined elastic half-planes. *J. Engng Mech. Div. ASCE* **88**, 10.

Eshelby, J. D. (1957). The determination of the elastic fields of an ellipsoidal inclusion and related problems. *Proc. R. Soc.* **A241**, 376–396.

Gao, Z. and Mura, T. (1989a). Evaluation of plastic damages from surface displacement data. *Int. J. Solids Structures* (submitted).

Gao, Z. and Mura, T. (1989b). On the inversion of residual stresses from surface displacements. *J. Appl. Mech.* (in press).

Lene, F. and Leguillon, D. (1982). Homogenized constitutive law for a cohesive composite material. *Int. J. Solids Structures* **18**, 443–458.

Mura, T. (1982). *Micromechanics of Defects in Solids*. Martinus Nijhoff.

Mura, T. and Furuhashi, R. (1984). The elastic inclusion with a sliding interface. *J. Appl. Mech.* **51**, 308–310.

Mura, T., Cox, B. and Gao, Z. (1986). Computer-aided nondestructive measurements of plastic strains from surface displacements. In *Computational Mechanics '86*, Tokyo, II (Edited by S. N. Atluri and G. Yagawa), Springer.

Mura, T., Jasiuk, I. and Tsuchida, E. (1985). The stress field of a sliding inclusion. *Int. J. Solids Structures* **16**, 1165–1179.

Muskhelishvili, N. I. (1963). *Some Basic Problems of the Theory of Elasticity*, 3rd edn. P. Noordhoff, Groningen, The Netherlands.

Tikhonov, A. N. (1963). The solution of ill-posed problems. *Doklady Akad. Nauk SSSR* **151**, 3.

APPENDIX A

Equation (19) can be obtained by following procedure. The configuration of our problem is shown in Fig. 1(a).

In equations (14) and (15), both $\mathbf{x}$ and $\mathbf{x}'$ vary on interface $|\Omega|$. Therefore, transformation of variables

$$\begin{aligned} \mathbf{x} = \mathbf{x}(\theta): &\quad x_1 = a_1 \sin\theta, \quad x_2 = a_2 \cos\theta \\ \mathbf{x}' = \mathbf{x}'(\varphi): &\quad x_1' = a_1 \sin\varphi, \quad x_2' = a_2 \cos\varphi, \quad 0 \leqslant \varphi, \theta \leqslant \pi \end{aligned} \tag{A1}$$

changes (14), (15) to

$$\int_0^\pi \Pi_{im}(\theta, \varphi) u_i(\theta)\, \mathrm{d}\theta - \int_0^\pi \Sigma_{im}(\theta, \varphi) t_i(\theta)\, \mathrm{d}\theta = 0, \quad 0 \leqslant \varphi \leqslant \pi \tag{A2}$$

$$\int_0^\pi \Pi^*_{im}(\theta, \varphi) u_i(\theta)\, \mathrm{d}\theta + \int_0^\pi \Pi^*_{im}(\theta, \varphi) b_i(\theta)\, \mathrm{d}\theta - \int_0^\pi \Sigma^*_{im}(\theta, \varphi) t_i(\theta)\, \mathrm{d}\theta = 0, \quad 0 \leqslant \varphi \leqslant \pi \tag{A3}$$

where the nature of θ and φ is shown in Fig. 1(b) and

$$\Pi_{im}(\theta, \varphi) = -0.5\delta_{im}\delta(\varphi-\theta)+\left\{C_{ijkl}G_{km,j}(\mathbf{x}, \mathbf{x}')\frac{ds}{d\theta}n_j\right\}\Big|\{\mathbf{x} = \mathbf{x}(\theta), \mathbf{x}' = \mathbf{x}'(\varphi)\} \tag{A4}$$

$$\Pi^*_{im}(\theta, \varphi) = -0.5\delta_{im}\delta(\varphi-\theta)+\left\{C^*_{ijkl}G^*_{km,j}(\mathbf{x}, \mathbf{x}')\frac{ds}{d\theta}n_j\right\}\Big|\{\mathbf{x} = \mathbf{x}(\theta), \mathbf{x}' = \mathbf{x}'(\varphi)\} \tag{A5}$$

$$\Sigma_{im}(\theta, \varphi) = G_{im}(\mathbf{x}, \mathbf{x}')\frac{ds}{d\theta}\Big|\{\mathbf{x} = \mathbf{x}(\theta), \mathbf{x}' = \mathbf{x}'(\varphi)\} \tag{A6}$$

$$\Sigma^*_{im}(\theta, \varphi) = G^*_{im}(\mathbf{x}, \mathbf{x}')\frac{ds}{d\theta}\Big|\{\mathbf{x} = \mathbf{x}(\theta), \mathbf{x}' = \mathbf{x}'(\varphi)\} \tag{A7}$$

$\delta(\varphi-\theta)$ in (A4) and (A5) is the Dirac delta function.

For equations (16) and (17), $\mathbf{x}$ varies on $|\Omega|$ and $\mathbf{x}'$ varies on the free surface $x'_1 = 0$, $x'_2 \in [-L, L]$. Therefore, we use

$$\begin{aligned}&\mathbf{x} = \mathbf{x}(\theta): \quad x_1 = a_1 \sin\theta, \quad x_2 = a_2\cos\theta,\\ &\mathbf{x}' = \mathbf{x}'(\varphi): \quad x'_2 = 0, x'_2 = \frac{2L}{\Pi}\varphi - L, \quad 0 \leqslant \varphi, \theta \leqslant \pi\end{aligned} \tag{A8}$$

which changes (16) and (17) to

$$\int_0^\pi \Gamma_{im}(\theta, \varphi)u_i(\theta)\,d\theta - \int_0^\pi \Delta_{im}(\theta, \varphi)t_i(\theta)\,d\theta = \begin{cases} u'_m(\varphi) & \varphi \notin \mathbf{R}\\ 0 & \varphi \in \mathbf{R}\end{cases} \tag{A9}$$

where $\mathbf{R} = [(L-a_2)\pi/2L, (L+a_2)\pi/2L]$, and

$$\int_0^\pi \Gamma^*_{im}(\theta, \varphi)u_i(\theta)\,d\theta + \int_0^\pi \Gamma^*_{im}(\theta, \varphi)h_i(\theta)\,d\theta - \int_0^\pi \Delta^*_{im}(\theta, \varphi)t_i(\theta)\,d\theta = \begin{cases} -u'_m(\varphi) & \varphi \in \mathbf{R}\\ 0 & \varphi \notin \mathbf{R}\end{cases} \tag{A10}$$

where θ and φ are indicated in Fig. 1(c) and

$$\Gamma_{im}(\theta, \varphi) = C_{ijkl}G_{km,j}(\mathbf{x}, \mathbf{x}')n_j\frac{ds}{d\theta}\Big|\{\mathbf{x} = \mathbf{x}(\theta), \mathbf{x}' = \mathbf{x}'(\varphi)\} \tag{A11}$$

$$\Delta_{im}(\theta, \varphi) = G_{im}(\mathbf{x}, \mathbf{x}')\frac{ds}{d\theta}\Big|\{\mathbf{x} = \mathbf{x}(\theta), \mathbf{x}' = \mathbf{x}'(\varphi)\}. \tag{A12}$$

The corresponding quantities for C^*_{ijkl}, $G^*_{km,j}$ are denoted by $\Gamma^*_{im}(\theta, \varphi)$ and $\Delta^*_{im}(\theta, \varphi)$. It should be noted that the transform $\mathbf{x}' = \mathbf{x}'(\varphi)$ in (A11) and (A12) is given in (A8) which is different from the one in (A1).

When we defined matrix $\mathbf{K}(\theta, \varphi)$ as

$$\mathbf{K}(\theta, \varphi) = \begin{Bmatrix} \Pi_{11} & \Pi_{21} & -\Sigma_{11} & -\Sigma_{21} & 0 & 0\\ \Pi_{12} & \Pi_{22} & -\Sigma_{12} & -\Sigma_{22} & 0 & 0\\ \Pi^*_{11} & \Pi^*_{21} & -\Sigma^*_{11} & -\Sigma^*_{21} & \Pi^*_{11} & \Pi^*_{21}\\ \Pi^*_{12} & \Pi^*_{22} & -\Sigma^*_{12} & -\Sigma^*_{22} & \Pi^*_{12} & \Pi^*_{22}\\ \Gamma_{11} & \Gamma_{21} & -\Delta_{11} & -\Delta_{21} & 0 & 0\\ \Gamma_{12} & \Gamma_{22} & -\Delta_{12} & -\Delta_{22} & 0 & 0\\ \Gamma^*_{11} & \Gamma^*_{21} & -\Delta^*_{11} & -\Delta^*_{21} & \Gamma^*_{11} & \Gamma^*_{21}\\ \Gamma^*_{12} & \Gamma^*_{22} & -\Delta^*_{12} & -\Delta^*_{22} & \Gamma^*_{12} & \Gamma^*_{22}\end{Bmatrix} \tag{A13}$$

then equation (19) is obtained from (A2), (A3), (A9) and (A10).

APPENDIX B

Let $0 \leqslant \gamma \leqslant \alpha$, $\mathbf{V}^\gamma(\theta)$ and $\mathbf{V}^\alpha(\theta)$ be solutions of (27) corresponding to the given parameters γ and α, respectively. Then, we have

$$\gamma\|\mathbf{V}^\alpha(\theta)\|^2 + \left\|\int_0^\pi \mathbf{K}(\theta, \varphi)\mathbf{V}^\alpha(\theta)\,d\theta - \mathbf{U}(\varphi)\right\|^2 \geqslant \gamma\|\mathbf{V}^\gamma(\theta)\|^2 + \left\|\int_0^\pi \mathbf{K}(\theta, \varphi)\mathbf{V}^\gamma(\theta)\,d\theta - \mathbf{U}(\varphi)\right\|^2 \tag{B1}$$

and

$$\alpha\|\mathbf{V}^{\alpha}(\theta)\|^2+\left\|\int_0^{\pi}\mathbf{K}(\theta,\varphi)\mathbf{V}^{\alpha}(\theta)\,d\theta-\mathbf{U}(\varphi)\right\|^2\leqslant\alpha\|\mathbf{V}^{\gamma}(\theta)\|^2+\left\|\int_0^{\pi}\mathbf{K}(\theta,\varphi)\mathbf{V}^{\gamma}(\theta)\,d\theta-\mathbf{U}(\varphi)\right\|^2. \tag{B2}$$

Therefore, when (B1) is subtracted from (B2) we have

$$(\alpha-\gamma)\|\mathbf{V}^{\alpha}(\theta)\|^2\leqslant(\alpha-\gamma)\|\mathbf{V}^{\gamma}(\theta)\|^2,$$

that is

$$\|\mathbf{V}^{\alpha}(\theta)\|^2\leqslant\|\mathbf{V}^{\gamma}(\theta)\|^2\quad\text{when }\gamma\leqslant\alpha. \tag{B3}$$

Furthermore, from (B1) and (B3),

$$f(\gamma)-f(\alpha)=\left\|\int_0^{\pi}\mathbf{K}(\theta,\varphi)\mathbf{V}^{\gamma}(\theta)\,d\theta-\mathbf{U}(\varphi)\right\|^2$$
$$-\left\|\int_0^{\pi}\mathbf{K}(\theta,\varphi)\mathbf{V}^{\alpha}(\theta)\,d\theta-\mathbf{U}(\varphi)\right\|^2\leqslant\gamma\{\|\mathbf{V}^{\alpha}(\theta)\|^2-\|\mathbf{V}^{\gamma}(\theta)\|^2\}\leqslant 0\quad\text{when }\gamma\leqslant\alpha.$$

The above equation indicates that $f(\alpha)$ is an increasing function.

Inequalities (29) and (30) can be obtained in the following way. As α goes to zero, the dominant terms in (27) are

$$\left\|\int_0^{\pi}\mathbf{K}(\theta,\varphi)\mathbf{V}^{\alpha}(\theta)\,d\theta-\mathbf{U}(\varphi)\right\|^2-\varepsilon$$

and the minimum is reached when $\mathbf{V}(\theta)$ is taken as the solution of (19). Therefore,

$$f(\alpha)=-\varepsilon<0,\quad\text{as }\alpha\to 0^+. \tag{B4}$$

As α goes to positive infinity, $\|\mathbf{V}(\theta)\|$ goes to zero in order to keep the term $\alpha\|\mathbf{V}(\theta)\|^2$ in (27) finite. Therefore

$$f(\alpha)=\|\mathbf{U}(\varphi)\|^2-\varepsilon>0,\quad\text{as }\alpha\to+\infty. \tag{B5}$$

The last inequality holds because ε, the error of displacement measurements, should be in lower order comparing with the displacements themselves.